This file is the final accepted version of the manuscript published in https://doi.org/10.1108/SASBE-01-2024-0014

LAND COVERAGE PREDICTION USING CONVOLUTIONAL NEURAL NETWORK FOR ENHANCED WIND LOADING ESTIMATION

Nasrollah Alinejad[a], Sungmoon Jung[a*], Jinglun Cai[b], Xiuwen Liu[b]

[a] Department of Civil and Environmental Engineering, FAMU-FSU College of Engineering, Tallahassee FL USA ([*] Corresponding author: sjung@eng.famu.fsu.edu)
[b] Department of Computer Science, Florida State University, Tallahassee FL USA

Abstract

Conventional land coverage prediction could not be used in wind engineering because it led to inaccurate surface roughness. This paper presents a new deep neural network for land coverage prediction that can distinguish low- and mid-rise buildings in the built environment, to enhance the estimation of surface roughness necessary in wind engineering. For the dataset, Landsat 8 satellite images were used. A patch-based convolutional neural network was employed and improved. The network predicted the land coverage at the center of the patch. Two different label schemes were used where the proposed network either achieved better accuracy than the conventional model, or recognized additional building types while maintaining a similar level of accuracy. The improvement of the proposed method will depend on the site characteristics. For the sites tested in this paper, the error reduction in wind speed and pressure was up to about 55%. In addition to more accurate wind speed and pressure, better identification of buildings will benefit wind engineering research as different building types cause different downwind effects.

Keywords

Remote sensing; land cover; neural network; CNN; wind; building;

1. Introduction

1.1. Land Coverage Prediction Using Neural Network

It has been decades since machine learning tools were applied to remote sensing problems. The early approaches include maximum likelihood classifier [1] and clustering [2], followed by more advanced techniques such as decision trees [3], random forests [3], neural networks [4], and support vector machines [5].

More recently, convolutional neural networks (CNN) led to significant progress in image classification. Due to the efficiency and effectiveness, CNN has also been applied to remote sensing image classification [6-8]. In Romero et al. [7], CNN was applied to seven images acquired with the Medium Resolution Imaging Spectrometer (MERIS) and achieved nearly 60% accuracy. In Castelluccio et al. [6], a pretrained GoogLeLeNet was applied to UCMerced [9], which

consisted of 2100 images; the CNN achieved 97% accuracy. As for pixel-based classification, a patch-based CNN was proposed by Sharma et al. [8] and was applied to a test site from the Florida Everglades area, resulting in 78% accuracy.

Typical CNN architectures consist of multiple layers of various types. Common types of layers are convolutional layer, pooling layer, feedforward layer, and softmax layer. Convolutional layers compute the convolution of the input image with kernels (also called filters). The kernels shift over input features and provide translation invariant responses. Pooling layers function as non-linear down-sampler and reduce the size of the input layer. There are non-linear functions to implement pooling, where max pooling is the most common. Pooling reduces the number of parameters to learn and provides some translation invariance. Feedforward layers are usually implemented after convolutional and pooling layers. They summarize the information provided by previous layers and support final decisions. The standard activation function for the output layer is softmax. Softmax layers are often viewed as a particular type of layers; however, they do not contain any training parameter.

1.2. Wind Engineering Applications of Predicted Land Coverage

Upstream terrain has a significant effect on wind pressure on buildings. Rougher land coverage will retard the wind more than smooth land, changing the wind loads. Wind tunnel testing is a standard method to investigate the effect of upstream surface roughness on wind loads on buildings [10, 11]. However, due to the difficulty of reproducing the complex real-world land coverage, investigations on upstream terrain effects have been limited to simple cases such as smooth to rough and rough to smooth roughness transitions [12-14].

In the real world, we are dealing with complex heterogeneous upstream terrain. The wind loading on a building is likely to deviate further from the known wind loading due to the complexity of the real-world land coverage. To address this issue, research is needed in two separate areas. First, wind tunnel testing needs to be conducted for more complex terrains. Thanks to the recent advance in wind tunnel testing techniques, researchers have begun to do so [10]. Second, research is needed to classify real-world land coverage with high accuracy, specifically for wind engineering applications. This paper deals with this second area of research.

The machine-learning-based land cover prediction is a promising technique because it can remove subjectivity in human interpretation. Such human interpretation was shown to be widely variable. Researchers and engineers generally “resorted to qualitative terms such as ‘suburban terrain’ or ‘open terrain with scattered obstructions’” [15], and therefore “the level of subjective interpretation is high” [16].

1.3. Knowledge Gap and Original Contribution

Despite the potential, wind engineers cannot yet employ machine-learning-based land cover prediction. The reason is that the past studies were intended for earth science, and accordingly, the land classification categories were primarily based on the differences in permeability. While useful for some engineering problems such as flooding, these land cover

categories alone cannot properly provide surface roughness. The error tends to be greater in developed areas such as urban and suburban, where most buildings exist.

This paper presents a new CNN for land coverage prediction that can distinguish low- and mid-rise buildings in the built environment. After presenting the training data, CNN, and its performance, we will illustrate how the new CNN improves the wind loading estimation.

2. Data Preparation

2.1. Site Selection

To train the network, we need to develop a dataset of sites that have various land coverages. In the U.S., dollar loss due to the wind has been shown to be closely correlated with exposure to hurricanes [17, 18]. Following the trajectory of major hurricanes in the past 20 years in the U.S., a total of 529 sites were selected proportional to a state's exposure to hurricanes. The sites in each state were manually selected such that different land coverages were present in the dataset. Table 1 shows the number of sites in each state. Table 2 shows the locations of sample sites.

Table 1: Selected states for the dataset and the number of sites in each state

State	Number of sites	State	Number of sites	State	Number of sites	State	Number of sites
Florida	50	Mississippi	20	Rhode Island	15	Indiana	10
Georgia	30	Maryland	20	West Virginia	10	Ohio	10
South Carolina	30	Delaware	20	Pennsylvania	10	Maine	10
North Carolina	30	New Jersey	20	Massachusetts	10	Vermont	10
Texas	30	Tennessee	15	New Hampshire	10	Oklahoma	10
Louisiana	25	Arkansas	15	Kentucky	10	New Mexico	5
Virginia	25	New York	15	Illinois	10	Arizona	5
Alabama	20	Connecticut	15	Missouri	10	California	4

Table 2: Attributes of 5 different sample sites

Site ID	State	City (nearby)	Latitude	Longitude
1	Florida	Miami	25.41191	-80.4964
51	Georgia	St Simons	31.15345	-81.3822
141	Texas	Kingsville	27.50718	-97.8191
351	New York	New York	40.97849	-72.1267
529	California	Santa Maria	34.85759	-120.419

2.2. Preparation of Input: Landsat 8 Data

The input to the network will be the satellite image. Landsat 8 [19] provides satellite images of the earth's surface with sufficient resolution to show different types of land cover such as developed areas, scrubs, forests, water, etc. Landsat 8 land imagery consists of 9 spectral bandwidths; however, we stacked bands 1 to 7 and band 9 in our network as these bands have the same resolution. See Table 3. The image data from Landsat 8 was obtained from the USGS website, and all images were from the 2016 version for consistency.

This file is the final accepted version of the manuscript published in https://doi.org/10.1108/SASBE-01-2024-0014

Table 3: Landsat 8 operational land imager information

Bands	Wavelength (μm)	Resolution (m)
Band 1: Coastal aerosol	0.43-0.45	30
Band 2: Blue	0.45-0.51	30
Band 3: Green	0.53-0.59	30
Band 4: Red	0.64-0.67	30
Band 5: Near Infrared	0.85-0.88	30
Band 6: SWIR 1	1.57-1.65	30
Band 7: SWIR 2	2.11-2.29	30
Band 9: Cirrus	1.36-1.38	30

Any image size could be used for the dataset as long as it was greater than the patch input to the network. See Figure 1. This research was part of a larger project where wind tunnel testing was needed. For convenience, the size of the image was determined as 3840 m × 3840 m so that a terrain for wind tunnel testing could be selected for any direction, as shown in Figure 2.

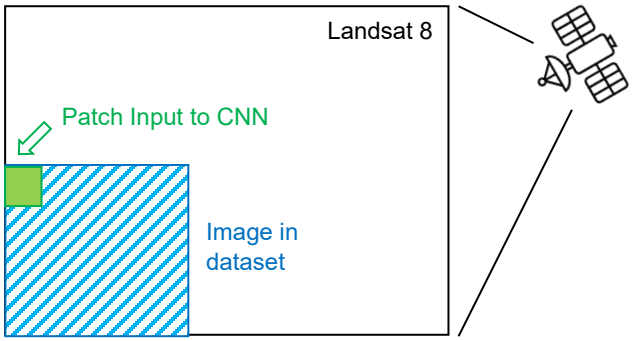

Figure 1: Relationship between the size of the image in the dataset, CNN input, and Landsat 8 (not to scale)

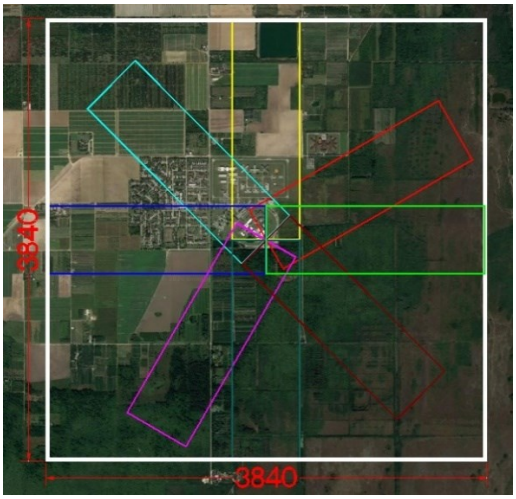

Figure 2: Selection of 1:100 scaled wind tunnel upstream fetch shown as colored rectangles (Google Earth image was used for this illustration instead of the Landsat 8, in order to show the terrain features better)

We developed a Python code to extract and store the 530 sites. Figure 3 shows a sample dataset. Since the size of the images is 3840 × 3840 m and the spatial resolution is 30 m, each image has 128 × 128 pixels.

This file is the final accepted version of the manuscript published in https://doi.org/10.1108/SASBE-01-2024-0014

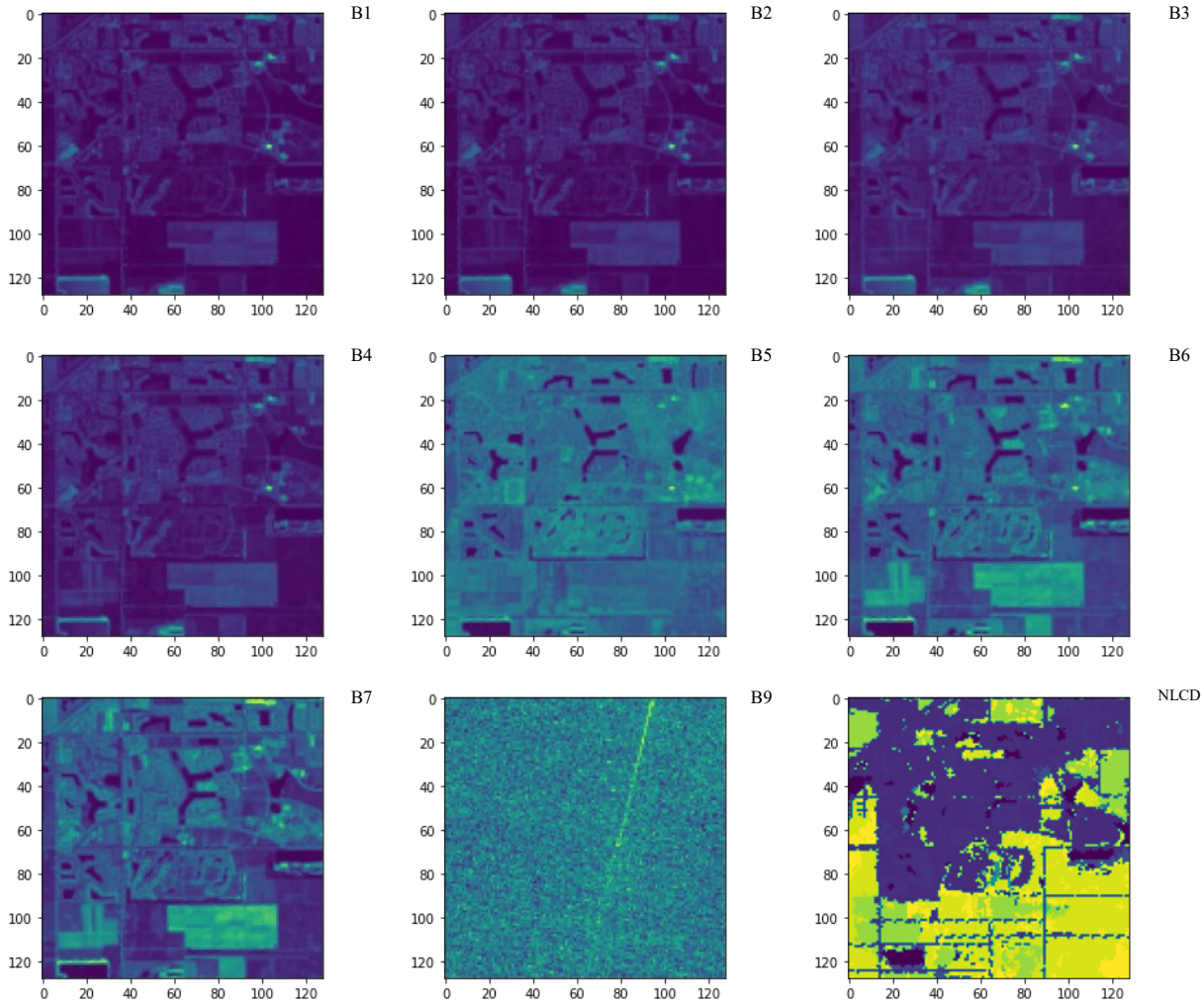

Figure 3: An example of Landsat 8 projection for bandwidths 1 to 7 and 9, respectively (site coordinates: Lat = 25.448995, Lon = -80.444257) and corresponding NLCD image (bottom right image)

2.3. Preparation of Output: Land Cover Labels

National Land Cover Database (NLCD) [20] is a Landsat-based dataset provided by USGS that captures different types of land cover and labels them into 20 categories, as shown in Table 4. The resolution of images in this dataset was 15 m. NLCD images were processed to obtain a land cover label for each pixel in the input data. The original land cover labels of the NLCD were consolidated in this research based on the surface roughness. For example, the NLCD classification has three different labels for the forest. However, all of them have similar roughness in wind engineering, and therefore only one label was used for them.

Table 4: NLCD-based land cover classification

NLCD Label	Land Cover	CNN Labels in this Research	z_0 range
11	Open Water	1	0.0001-0.0005
12	Perennial Ice, Snow		
21	Developed, Open Space	2	0.3-0.7
22	Developed, Low Density		

This file is the final accepted version of the manuscript published in https://doi.org/10.1108/SASBE-01-2024-0014

23	Developed, Medium Density		
24	Developed, High Density		
31	Barren Land	3	0.001-0.005
41	Deciduous Forest	4	1-2.3
42	Evergreen Forest		
43	Mixed Forest		
51	Dwarf Scrub	5	0.0024-0.005
52	Shrub Scrub		
71	Grassland, Herbaceous	6	0.005-0.01
81	Cultivated Corps		
72	Sedge, Herbaceous	7	0.002-0.007
73	Lichens		
74	Moss		
82	Pasture, Hay		
90	Woody Wetlands	8	0.001-0.003
95	Emergent Herbaceous Wetland		

As shown in Table 4, NLCD classifies developed areas based on density. In affecting the wind, the surface of the building facing the wind has the greater effect — a tall building will retard the wind greater than a low-rise building. In addition, other obstacles such as trees exist close to the surface, whereas a tall building will immediately face the wind in general. In order to consider the greater retardation effect by taller buildings, the built area was further divided into two different labels as shown in Table 5.

Table 5: Improved land cover classification for developed areas

NLCD-Based Land Cover	Improved Land Cover	CNN Labels in this Research
Developed, Open Space; Low Density; Medium Density; High Density	Developed, Low-rise buildings	2
	Developed, Mid-rise buildings	9

In order to improve the NLCD classification of developed areas, we had to review all sites using Google Earth and manually identify the mid-rise buildings. Buildings with 3 stories or fewer were considered as low-rise building, whereas buildings with at least four stories or more were considered as mid-rise buildings. Figure 4 shows an example of how the classification of a site was improved by identifying a mid-rise building.

(a) (b)

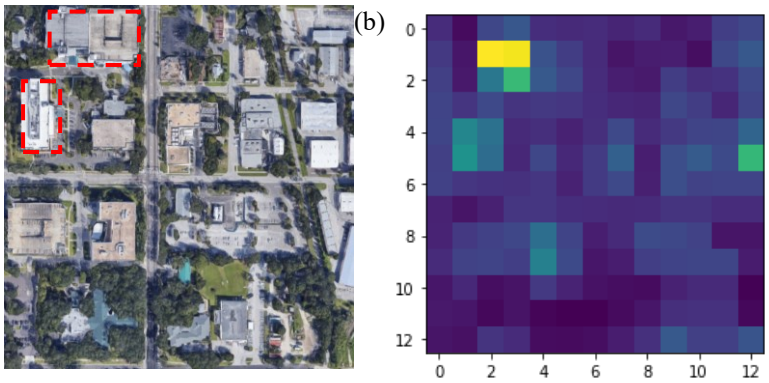

This file is the final accepted version of the manuscript published in https://doi.org/10.1108/SASBE-01-2024-0014

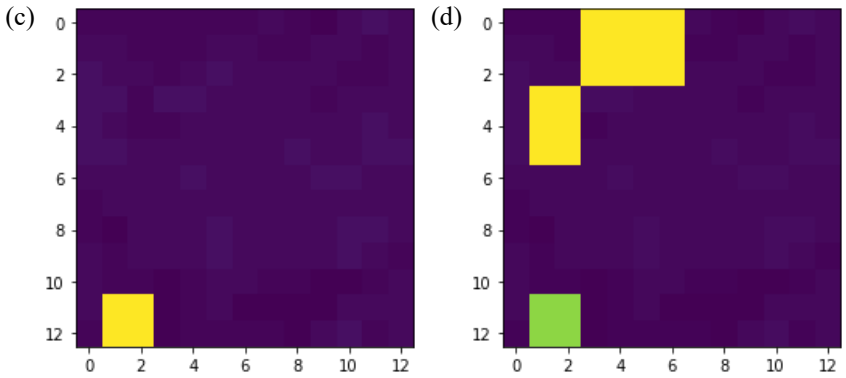

Figure 4: (a) Aerial image of the site ID #37 with Lat = 27.949945and Lon = -82.797666 with two mid-rise buildings outlined with dashed red line rectangles, (b) Bandwidth 2 of Landsat 8 image for the same site, (c) Original NLCD image of the site, (d) Improved classification considering the mid-rise building

2.4. Data Storage

The Landsat 8 images and land cover classification were stored in the list. Each list corresponds to each pixel, i.e., a 30 m × 30 m land. The arrays of the list contained the site ID, bandwidth number, and pixel X and Y coordinates. The second array of the list had the 8 different bandwidths of Landsat 8 images and the land cover label. The first 8 entries of the second array were the input to the CNN, whereas the last entry was the output of the CNN prediction of the land coverage label.

3. Deep Convolutional Neural Network for Land Coverage Prediction

3.1. The Architecture of the Neural Network and Training Parameters

Patch-based inputs were used for the CNN. The optimal patch size depends on the remote sensing imagery source. After training and testing the performance of different patch sizes, the patch size in this research was determined as 15 × 15. Therefore, for each pixel where the CNN was to predict the land coverage, 15 × 15 × 8 input patch was used where the 8 corrresponds to 8 different bandwidths of the satellite image.

We chose a ratio of 9:1 for the training and validation data. As a result, 7.3 million and 0.8 million samples were obtained for the training and validation data, based on the 530 sites, their size and the patch size of 15 × 15.

The CNN architecture is based on the patch-based CNN proposed in Sharma et al. [8]. The main differences and improvements are that our CNN has a batch normalization layer, dropout mechanism, modified kernel size, and layer width hyperparameters. In our patched-based CNN, pooling has not been adopted because of limited improvement of the performance for the small patch size used in this research.

This file is the final accepted version of the manuscript published in https://doi.org/10.1108/SASBE-01-2024-0014

The proposed CNN consists of eight layers, as shown in Figure 5. A batch normalization was used for the first layer. Batch normalization standardizes input data more effectively than other conventional standardization methods. The batch normalization layer transformed the input to maintain the mean and standard deviation output close to 0 and 1, respectively. Thus, the mean and variance initializers were set to 0 and 1, correspondingly, with the momentum of 0.99. After the batch normalization, five convolutional layers were added. A fixed kernel size of 3×3 and stride value of 1 were used for all convolutional layers. The dropout rate was 0.1. The L1 regularization was used in each convolutional layer. The first four convolutional layers had 64 filters, and the last convolutional layer had 32 filters. Note that a significantly larger number of filters were used than the patch-based CNN in Sharma et al. [8]. The number of filters was adapted to our dataset, which covers a wider range of locations with a more diverse land cover. The feedforward layer had a width of 3200. The final output layer was softmax, a commonly used standard for classification tasks. The loss function for the proposed model was cross-entropy. The training was conducted using ADAM optimizer [21] with a learning rate of 0.0003.

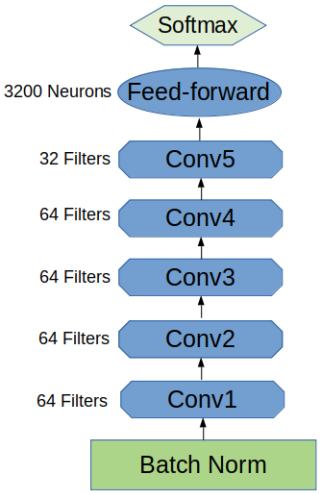

Figure 5: Convolutional Neural Network architecture used in this research

3.2. Accuracy of the Base Model

The input to the network was always the 15 × 15 × 8 patch from the Landsat 8. Two different label types were used for the output. The network trained with the first label type is discussed in this section, termed as the "base model." The CNN was trained using the NLCD-based dataset shown in Table 4, for 20 epochs (120000 steps). Instead of the original NLCD labels shown in the first column, surface roughness-based labels in the third column were used. Figure 6 shows the change of loss (left) and the classification accuracy (right) on the training data. The initial loss value at step 1000 was around 0.75 and it stabilized around 0.13 after 120000 steps. The classification accuracy for the training set achieved 95% at the end of training.

While the patch-based CNN developed by Sharma et al. [8] was able to achieve a validation accuracy of 78%, our model improved the validation accuracy to 90%. Figure 7 shows the confusion matrix of model prediction on the validation set.

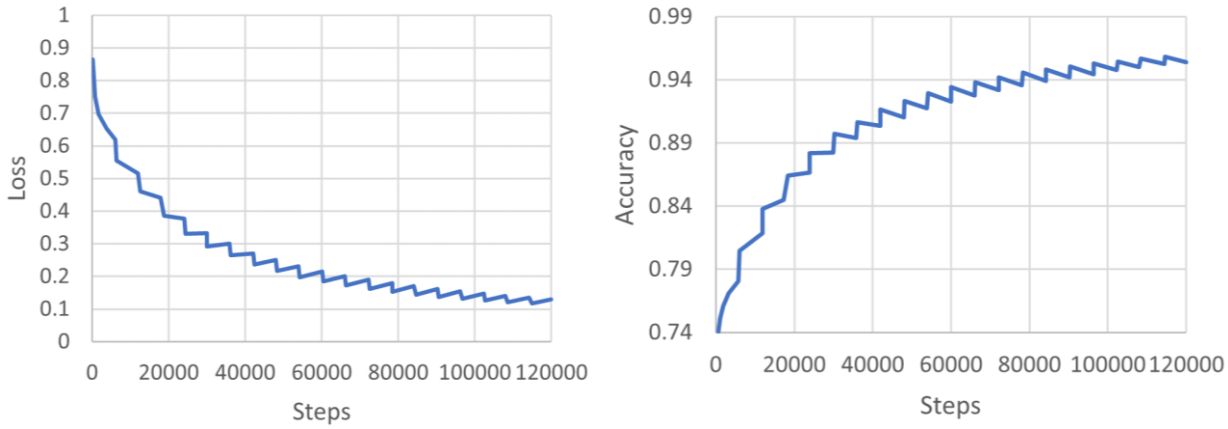

Figure 6: Training loss (left) and accuracy (right) of the network

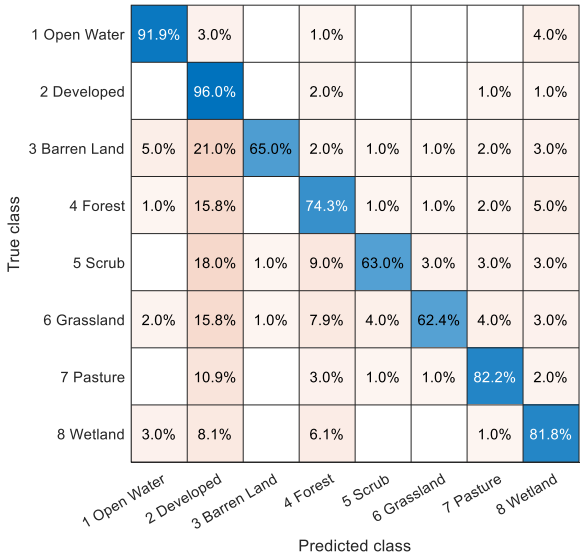

Figure 7: Confusion matrix on validation set

As an illustration of CNN prediction, we selected a location (site ID = 521, site coordinates: Lat = 34.923829, Lon = -110.137571) in Holbrock, AZ, and displayed the classification outputs of the model together with the target labels as shown in Figure 8.

This file is the final accepted version of the manuscript published in https://doi.org/10.1108/SASBE-01-2024-0014

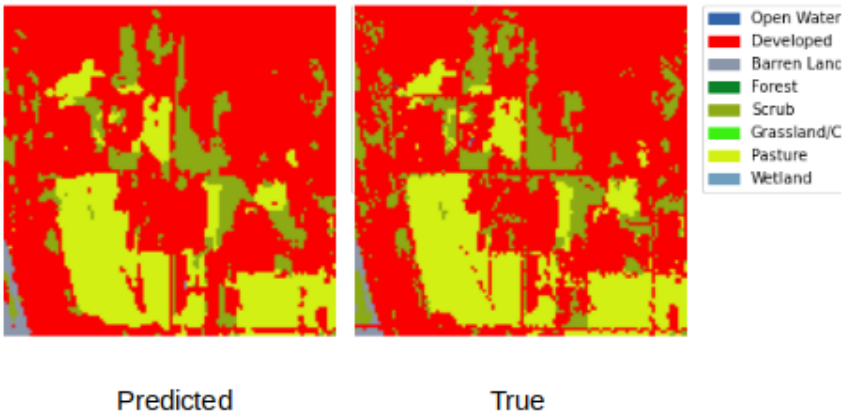

Figure 8: Sample CNN prediction for site ID #521: from the validation set

3.3. Comparison with other known algorithms

Here, we compared the accuracy of the base model with random forest and support vector machine algorithms. The random forest algorithm was trained with 100 estimators (trees) and maximum depth of 10. The input dataset was the same as previous section. At the end of training, the accuracy of random forest algorithm on the validation set was 62.0 %. The increase in the number of estimator did not change the accuracy considerably. The accuracy was 62.1 % with 200 esyimator. The linear support vector machine with maximum iteration of 200 with regularization parameter of 1 (C = 1) achieved 61.9 % accuracy on the validation set with the same input dataset. Compared with the proposed model with 95% accuracy, both random forest and support vector machine algorithms did not achived a good accuracy.

3.4. Accuracy of the Refined Model

The network trained with the second label type is discussed in this section, termed as the "refined model." The second label type changed the developed area labels from Table 4 to Table 5. The CNN was trained for 20 epochs (120000 steps). The trend in loss and accuracy were similar to the base model shown in Figure 6. While the base model was able to achieve the validation accuracy of 90%, the refined model had the validation accuracy of 80% due to the increased difficulty with additional labels.

The refined model improves prediction of labels in developed areas, and therefore, will have a major impact on the estimation of wind speed and pressure. Instead of just showing the CNN prediction of labels alone, the prediction along with the impact on the wind speed and pressure will be discussed in the next section.

4. Improvement in Wind Speed and Pressure Estimation

4.1. Relevant Theory

This file is the final accepted version of the manuscript published in https://doi.org/10.1108/SASBE-01-2024-0014

This section will discuss the improvement in wind speed and pressure estimation, due to the improved land cover classification by the proposed method. The earth's surface slows the wind and creates turbulence. The resulting mean wind speed near surface can be described by the log law:

$$V_z = \frac{u_*}{\kappa} \ln\left(\frac{z}{z_0}\right) \quad (1)$$

where V_z is the mean wind speed at height z, u_* is the friction velocity, κ is the von Karman constant, and z_0 is the roughness length. The pressure at a point Q of the building can be obtained from the following:

$$p(Q) = \frac{1}{2}\rho V_z^2 C_p(Q) \quad (2)$$

where ρ is the air density, and C_p is the pressure coefficient at this point. Further details have been removed for the brevity of the discussion. Finally, the effective roughness length (z_{0e}) for the given terrain will be computed using the Taylor's method [22]:

$$\ln z_{0e} = \langle \ln z_0 \rangle + a_1\{\langle (\ln z_0)^2 \rangle - (\langle \ln z_0 \rangle)^2\} \quad (3)$$

where $\langle \cdot \rangle$ denotes an area-weighted logarithmic average, z_0 is the roughness length of each grid cell, and a_1 is the coefficent that depends on the Rossby number [22].

4.2. Testing Cases

To quanitfy the improvement by the proposed method, three testing sites were selected, as shown in Figure 9. The sites were selected so that they cover three distinctive effective roughness lengths. According to the ASCE 7, the typical surface roughness of Exposures D, C, and B are $z_0 = 0.005$, 0.02, and 0.3 m, respectively [23]. To select sites similar to $z_0 = 0.005$ and 0.02, the sites that had the closest effective z_0 were chosen from the training set. On the other hand, due to the small number of sites that had mid-rise buildings, the site for $z_0 = 0.3$ was chosen manually. The effective z_0 for the three testing sites were 0.0029, 0.0224, and 0.536 m, respectively. The z_0 calculation used the median value for each category shown in Table 4.

(a) 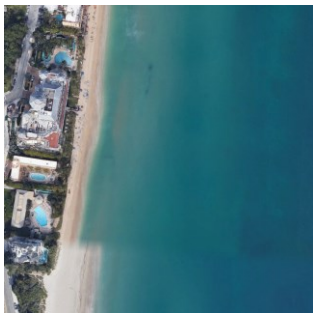 (b) 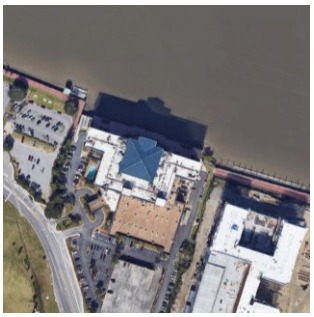 (c) 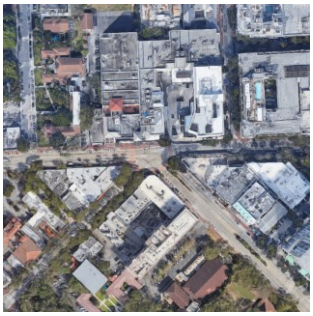

Figure 9: Three testing sites to quantify the improvement in wind speed and pressure: (a) effective z_0 = 0.0029 m, (b) effective z_0 = 0.0224 m, (c) effective z_0 = 0.536 m (Google Earth image was used for this illustration instead of the Landsat 8, in order to show the terrain features better)

This file is the final accepted version of the manuscript published in https://doi.org/10.1108/SASBE-01-2024-0014

The size of the testing sites was determined as 300 m by 300 m based on past studies that the peak wind loads were dominated by a short distance upwind terrain up to 300-400 m [16, 24, 25]. The size corresponds to 10 × 10 pixels. In the examples below, the wind speed and pressure improvement will be computed for the standard height of $z = 10$ m.

4.3. Improvement Compared to the Conventional Land Cover Prediction

The conventional land cover prediction utilizes the original NLCD labels (Table 4, column 1), with a validation accuracy of 78% [8]). The proposed method, the Base Model, had a validation accuracy of 90%, thanks to the improvements made in this study as well as the consolidation of labels with similar surface roughness.

The following approach was used to quantify the improvement in wind speed and pressure estimation. The testing site had 10 × 10 = 100 pixels, with each pixel representing a certain land cover. To quantify the effect of the classification error in the conventional approach, 100 – 78 = 22%, or 22 pixels, were randomly selected and assigned with a random misclassification. Next, the effective surface roughness was calculated using Equation (3), followed by the estimation of wind speed and pressure using Equations (1) and (2). The error compared to the correct classification was computed. The simulation was repeated 10,000 times. The Base Model was tested similarly but using 100 – 90 = 10% random misclassification.

Figure 10 and Figure 11 show the improvement in wind speed and pressure estimation when the proposed method was used. For $z_0 = 0.0029$ site, the proposed method decreased the error mean from –6.1% to –2.9% (53.3% reduction) for velocity, and from –11.8% to –5.6% (52.7% reduction) for pressure. The standard deviation also had a 27.0% reduction for velocity and a 24.6% reduction for pressure. For z_0 = 0.0224 m site, the error mean changed from +0.75% to +0.33% (56.2% reduction) for velocity, and from +1.65% to +0.73% (55.9% reduction) for pressure. The standard deviation error reduction was 30.4% for velocity and 30.9% for pressure.

For the sites tested, the percentage reduction in error was comparable for both sites, but z_0 = 0.0029 m site error reduction was more significant in terms of magnitude. The error reduction magnitude will depend on the distribution of land coverage — See Table 4, z_0 range for various land coverages.

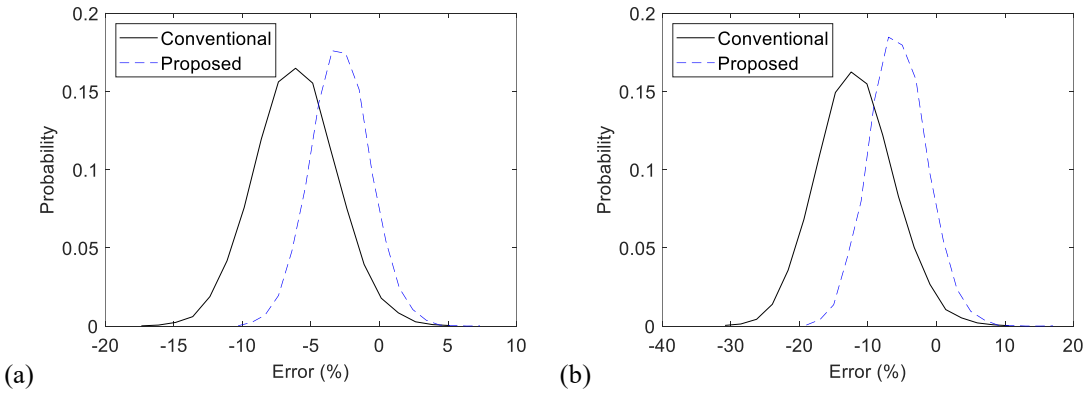

This file is the final accepted version of the manuscript published in https://doi.org/10.1108/SASBE-01-2024-0014

Figure 10. Improvement by the proposed method in estimating (a) wind speed and (b) pressure, effective z0 = 0.0029 m

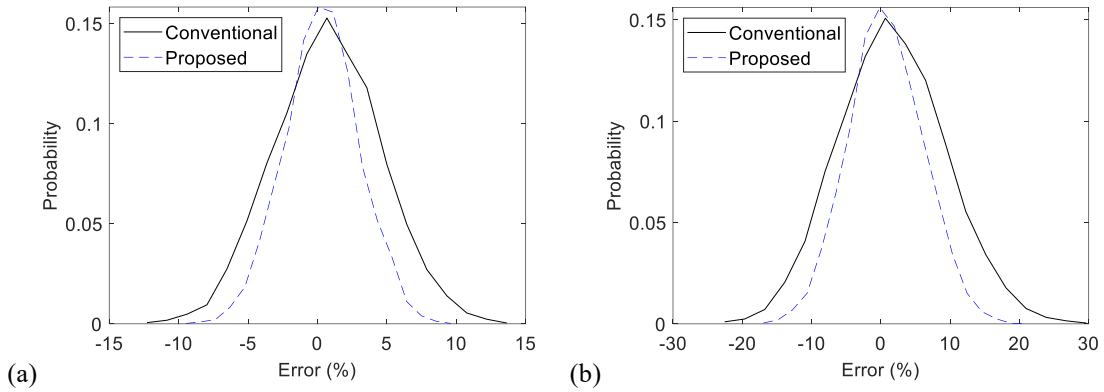

Figure 11. Improvement by the proposed method in estimating (a) wind speed and (b) pressure, effective z_0 = 0.0224 m

4.4. Improvement Between the Base Model and the Refined Model

Next, we discuss the improvement between the Base Model and the Refined Model. The testing was conducted for the z_0 = 0.536 m case because the refinement would be most distinctive in a relatively high roughness site. In comparing the Base Model and the Refined Model, unlike the previous section where the comparison was made with other researchers' work, the actual CNN prediction could be used.

Figure 12 compares the true labels, prediction by the Base Model, and prediction by the Refined Model. The z_0 is equal to 0.506 m for the prediction by the Base model and 0.513 m for the prediction by the Refined model. Although the contribution to the effective z_0 is small, since the wind flow and pressure will be significantly affected by immediate upwind terrain and surrounding buildings [26-27], our prediction can help identify such cases.

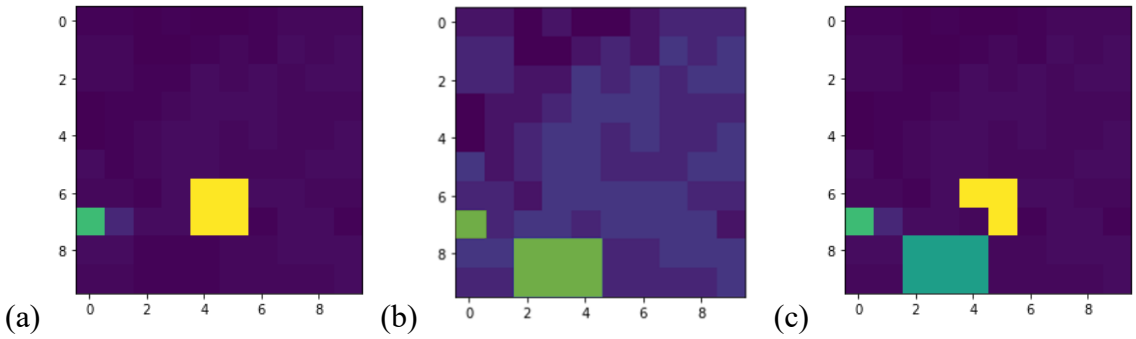

Figure 12. Comparison of the CNN prediction of a site with buildings: (a) target labels showing low- and mid-rise buildings, (b) Base Model prediction, (c) Refined Model prediction
Blue = low-rise building, Yellow = mid-rise building, Green = grassland

5. Conclusions

Machine-learning-based land cover prediction methods have not been used by wind engineers because the available methods were intended for earth science. Such methods could not properly provide surface roughness. This paper presents a new deep neural network for land coverage prediction that can distinguish low- and mid-rise buildings in the built environment, to enhance the estimation of surface roughness necessary in wind engineering.

To train and test the network, Landsat 8 satellite images were used. The 8 bandwidths that had 30 m resolution were used. A patch-based CNN was employed and improved. The patch size was 15 × 15 × 8. The CNN predicted the land coverage at the center of the 15 × 15 pixels. First, the conventional NLCD-based labels were improved for wind engineering applications. Next, additional categories were added along with manual data preparation to improve the prediction of different buildings.

Compared to the validation accuracy of 78% in a previous study [8], the proposed method achieved the validation accuracy of 90% thanks to the improvements made in this study as well as the consolidation of labels with similar surface roughness. When additional building categories were added, the validation decreased to 80%, which is comparable to the previous study but is now able to predict different building types.

After developing the CNN, we quantified the improvement in estimating the wind speed and pressure. The improvement of the proposed method will depend on the site characteristics. For the sites tested in this paper, the error reduction in wind speed and pressure was up to about 55%. In addition to more accurate wind speed and pressure, better identification of buildings will benefit wind engineering research as different building types cause different downwind effects. An example application would be automated recognition of areas that have a certain distance from the target building type to identify downwind areas affected by high winds.

Acknowledgments

This material is based upon work supported by the National Science Foundation under Grant No. CMMI-1856205. Any opinions, findings, and conclusions or recommendations expressed in this material are those of the authors and do not necessarily reflect the views of the National Science Foundation.

References

1. Strahler, A.H., *The use of prior probabilities in maximum likelihood classification of remotely sensed data.* Remote sensing of Environment, 1980. **10**(2): p. 135-163.
2. Huang, K.-Y., *A synergistic automatic clustering technique (SYNERACT) for multispectral image analysis.* Photogrammetric engineering and remote sensing, 2002. **68**(1): p. 33-40.
3. Xu, M., P. Watanachaturaporn, P.K. Varshney, and M.K. Arora, *Decision tree regression for soft classification of remote sensing data.* Remote Sensing of Environment, 2005. **97**(3): p. 322-336.
4. Kavzoglu, T. and P.M. Mather, *The use of backpropagating artificial neural networks in land cover classification.* International journal of remote sensing, 2003. **24**(23): p. 4907-4938.

5. Mountrakis, G., J. Im, and C. Ogole, *Support vector machines in remote sensing: A review.* ISPRS Journal of Photogrammetry and Remote Sensing, 2011. **66**(3): p. 247-259.
6. Castelluccio, M., G. Poggi, C. Sansone, and L. Verdoliva, *Land use classification in remote sensing images by convolutional neural networks.* arXiv preprint arXiv:1508.00092, 2015.
7. Romero, A., C. Gatta, and G. Camps-Valls, *Unsupervised deep feature extraction for remote sensing image classification.* IEEE Transactions on Geoscience and Remote Sensing, 2015. **54**(3): p. 1349-1362.
8. Sharma, A., X. Liu, X. Yang, and D. Shi, *A patch-based convolutional neural network for remote sensing image classification.* Neural Networks, 2017.
9. Yang, Y. and S. Newsam. *Bag-of-visual-words and spatial extensions for land-use classification*. in *Proceedings of the 18th SIGSPATIAL international conference on advances in geographic information systems*. 2010.
10. Fernández-Cabán, P. and F. Masters, *Near surface wind longitudinal velocity positively skews with increasing aerodynamic roughness length.* Journal of Wind Engineering and Industrial Aerodynamics, 2017. **169**: p. 94-105.
11. Ferreira, L.M., G. Amirinia, and S. Jung, *Surface pressure distribution on patterned cylinders under simulated atmospheric boundary layer winds.* The Structural Design of Tall and Special Buildings, 2017.
12. Deaves, D., *Computations of wind flow over changes in surface roughness.* Journal of Wind Engineering and Industrial Aerodynamics, 1981. **7**(1): p. 65-94.
13. Tieleman, H., *Wind characteristics in the surface layer over heterogeneous terrain.* Journal of Wind Engineering and Industrial Aerodynamics, 1992. **41**(1-3): p. 329-340.
14. Wang, K. and T. Stathopoulos, *Exposure model for wind loading of buildings.* Journal of Wind Engineering and Industrial Aerodynamics, 2007. **95**(9): p. 1511-1525.
15. Irwin, P.A., *Exposure categories and transitions for design wind loads.* Journal of Structural Engineering, 2006. **132**(11): p. 1755-1763.
16. Stathopoulos, T., K. Wang, and I. Zisis. *Wind loading and building exposure: Are we still on A, B, C?* in *Structures Congress 2009: Don't Mess with Structural Engineers: Expanding Our Role*. 2009.
17. Kakareko, G., S. Jung, O.A. Vanli, A. Tecle, O. Khemici, and M. Khater, *Hurricane loss analysis based on the population-weighted index.* Frontiers in Built Environment, 2017. **3**: p. 46.
18. Pielke Jr, R.A., J. Gratz, C.W. Landsea, D. Collins, M.A. Saunders, and R. Musulin, *Normalized hurricane damage in the United States: 1900–2005.* Natural Hazards Review, 2008. **9**(1): p. 29-42.
19. Roy, D.P., M. Wulder, T.R. Loveland, C. Woodcock, R. Allen, M. Anderson, D. Helder, J. Irons, D. Johnson, and R. Kennedy, *Landsat-8: Science and product vision for terrestrial global change research.* Remote sensing of Environment, 2014. **145**: p. 154-172.
20. Homer, C., J. Dewitz, L. Yang, S. Jin, P. Danielson, G. Xian, J. Coulston, N. Herold, J. Wickham, and K. Megown, *Completion of the 2011 National Land Cover Database for the conterminous United States–representing a decade of land cover change information.* Photogrammetric Engineering & Remote Sensing, 2015. **81**(5): p. 345-354.
21. Kingma, D.P. and J. Ba, *Adam: A method for stochastic optimization.* arXiv preprint arXiv:1412.6980, 2014.
22. Taylor, P.A., *Comments and further analysis on effective roughness lengths for use in numerical three-dimensional models.* Boundary-layer meteorology, 1987. **39**(4): p. 403-418.
23. ASCE, *Minimum Design Loads for Buildings and Other Structures*. 2022, Reston, VA: American Society of Civil Engineers.
24. Wang, K. and T. Stathopoulos. *The impact of exposure on wind loading of low buildings*. in *Structures Congress 2006: Structural Engineering and Public Safety*. 2006.
25. Zisis, I. and T. Stathopoulos. *Wind loads on low-rise buildings: Upstream exposure effect*. in *7th Asia-Pacific Conf. on Wind Engineering*. 2010.

26. C.-H. Chang and R. N. Meroney, *The effect of surroundings with different separation distances surface pressures on low-rise buildings,* Journal of Wind Engineering and Industrial Aerodynamics, vol. 91, pp. 1039-1050, 2003.

27. Y. C. Kim, A. Yoshida, and Y. Tamura, *Characteristics of surface wind pressures on low-rise building located among large group of surrounding buildings,* *Engineering Structures,* vol. 35, pp. 18-28, 2012.